Probing the equation of state with pions

Qingfeng Li [1*] , Zhuxia Li [2] , Sven Soff [3], Marcus Bleicher [3], and Horst Stöcker [1,3]

1) Frankfurt Institute for Advanced Studies (FIAS),

Johann Wolfgang Goethe-Universität,

Max-von-Laue-Str. 1,

D-60438 Frankfurt am Main, Germany

2) China Institute of Atomic Energy,

P.O. Box 275 (18),

Beijing 102413, P.R. China

3) Institut für Theoretische Physik,

Johann Wolfgang Goethe-Universität,

Max-von-Laue-Str. 1,

D-60438 Frankfurt am Main, Germany

[*] Fellow of the Alexander von Humboldt Foundation.

Abstract

The influence of the isospin-independent, isospin- and momentum-dependent equation of state (EoS), as well as the Coulomb interaction on the pion production in intermediate energy heavy ion collisions (HICs) is studied for both isospin-symmetric and neutron-rich systems. The Coulomb interaction plays an important role in the reaction dynamics, and strongly influences the rapidity and transverse momentum distributions of charged pions. It even leads to the π^-/π^+ ratio deviating slightly from unity for isospin-*symmetric* systems. The Coulomb interaction between mesons and baryons is also crucial for reproducing the proper pion flow since it changes the behavior of the directed and the elliptic flow components of pions visibly.

The EoS can be better investigated in neutron-rich system if *multiple* probes are measured simultaneously. For example, the rapidity and the transverse momentum distributions of the charged pions, the π^-/π^+ ratio, the various pion flow components, as well as the *difference* of π^+-π^- flows. A new sensitive observable is proposed to probe the symmetry potential energy at high densities, namely the transverse momentum distribution of the elliptic flow difference $[\Delta v_2^{\pi^+-\pi^-}(p_t^{\rm c.m.})]$.

PACS numbers: 24.10.Lx, 25.75.Dw, 25.75.-q

I. INTRODUCTION

Intermediate energy heavy ion collisions (HICs) are closely connected to the investigation of the nuclear equation of state (EoS). One of the main issues is to pin down the incompressibility ($K_{\rm NM}$) of nuclear matter. Although many efforts have been pursued in the past few decades this problem is still far from being solved thoroughly (see, for example, Refs. [1, 2]). Furthermore, the symmetry energy [3, 4, 5, 6] for isospin-asymmetric matter, the momentum dependence [7, 8, 9, 10, 11, 12] of the EoS, have also been found to be very important for the dynamics of the intermediate energy HICs and make the problem of probing the EoS even more complex.

In order to explore explicitly the incompressibility, the isospin dependence and the momentum dependence of the EoS, sensitive probes were put forward, however, mostly individually. Nevertheless, sensitive probes are not always proprietary, that is, they might be affected not only by single physical quantity. Therefore, it is quite necessary to explore multiple probes simultaneously so that the comparison between the experimental data and the corresponding theoretical predictions becomes more consistent.

In addition to free nucleons and light fragments, probes related to pions such as the π^-/π^+ ratio and the directed and elliptic flows, have been proven to be very useful to test the reaction dynamics as well as the EoS [10, 12, 13, 14, 15, 16, 17, 18, 19, 20, 21]. It was supposed and observed in Refs. [10, 19, 22] that pions show a weak positive flow effect in central collisions while a weak antiflow effect in peripheral collisions due to the shadowing effect of spectators. It should be mentioned that experimental measurements on the pion production with various collision systems and beam energies have been released by the FOPI/GSI Collaboration in recent years, for example, see Refs. [23, 24], which indeed largely deepen our insight into the production mechanism of pions in intermediate energy HICs, as well as the dynamics of the nuclear reaction itself.

In this work we will study a variety of observables related to pion production in isospin-symmetric and -asymmetric systems from central and semi-peripheral intermediate-energy HICs. The microscopic transport model - ultrarelativistic quantum molecular dynamics (UrQMD) [25, 26, 27, 28] - is adopted with an update of the potentials in the mean field part.

The paper is arranged as follows. In section II, we briefly introduce the UrQMD model

and the improvements of the potentials in the mean field part. In section III, the results of the ratios between the yields of charged pions, the various directed and elliptic flows of pion mesons are shown and discussed. Finally, a summary is given in section IV.

II. THE URQMD TRANSPORT MODEL AND THE POTENTIAL UPDATE

In the UrQMD transport model [25, 26], the initialization of projectile and target nuclei, the equation of motion of hadrons, and the collision term are described microscopically. This model was designed at the beginning for simulating HICs in the energy range from SIS to RHIC, where the contribution of nuclear mean field potentials to the dynamics of the reaction is considered to be weak. It is known that the conventional (or isospin-dependent) quantum molecular dynamics (QMD) model [10, 29] is mainly applied to the (isospin-asymmetric) intermediate-energy HICs. The UrQMD model inherits the basic treatment of the baryonic equation of motion in the QMD model, thus, after introducing some modern ingredients for the mean field part, it is believed that the UrQMD model can also be used to properly describe the physical phenomena in HICs at intermediate energies.

Furthermore, it has been seen that the contribution of the mean field to the reaction dynamics can not simply be neglected at SIS and even AGS energies [18, 30]. It was shown in Ref. [30] that the experimental elliptic flow as a function of beam energy ranging from $2-10A$ GeV for midrapidity protons in Au+Au collisions can be only successfully described if mean field potentials are taken into account, while pure cascade calculations fail. In Ref. [18] it has been shown that the potential that Σ hyperons encounter in the nuclear medium plays an important role in their evolution process in HICs at SIS energies. Thus, we have updated the potential interactions in the UrQMD model for the intended studies.

In addition to the isospin- and momentum- independent terms originally implemented in the mean field part of the UrQMD model, the following contributions are also considered here:

1. The contribution of the Coulomb interaction between *mesons* and hadrons (mesonic Coulomb potential) are supplied in addition to the Coulomb interaction between two baryons (baryonic Coulomb potential), in total, we call it hadronic Coulomb potential. It has been found that the Coulomb interaction between baryons and charged π mesons plays an essential role in the dependence of the π^-/π^+ ratios on rapidity and transverse momentum [17, 23, 24].

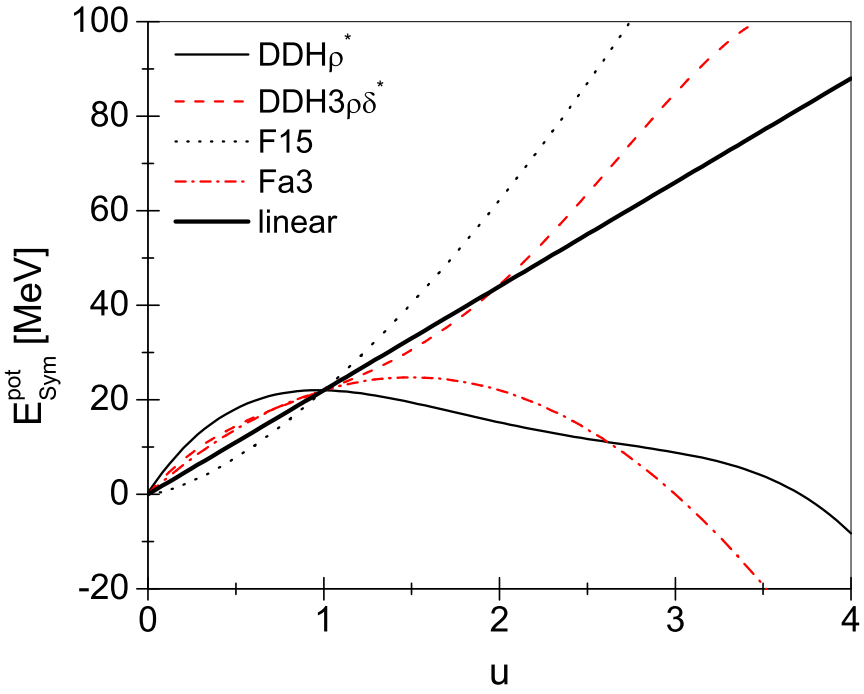

FIG. 1: Parametrizations of the nuclear symmetry potential energy DDHρ^*, DDH3$\rho\delta^*$, F15, and Fa3, as well as a linear one as a function of the reduced density u.

2. Like in our previous work [17, 18], the symmetry potentials of all baryons, i.e., the nucleons, the $\Delta(1232)$s, the $N^*(1440)$s, and the hyperons Λ and Σ, are introduced. Four density-dependent parameterizations for symmetry potential energy are considered: (1) u^γ with $\gamma = 1.5$ (called F15). Here $u = \rho/\rho_0$ is the reduced nuclear density; (2) $u\cdot(a-u)/(a-1)$ with $a = 3$ (Fa3). a is the so-called reduced critical density [31]; (3) and (4) so-called DDHρ^* and DDH3$\rho\delta^*$ symmetry potential energies, which are inspired by the relativistic mean-field calculations of DDHρ and DDH3$\rho\delta$ [32]. The symmetry energy coefficient $S_0 = 34$ MeV is adopted [1, 33]. The density dependence of the symmetry potential energies adopted is shown in Fig. 1. One sees from Fig. 1 that for reduced densities $u < 1$, DDH3$\rho\delta^*$ is very close to Fa3, both lie between DDHρ^* and F15. For $u > 1$, their density dependences are rather different: for $1 < u < 2.6$, the order of the symmetry potential energy $E_{\rm sym}^{\rm pot}$ is F15 $>$ DDH3$\rho\delta^*$ $>$ Fa3 $>$ DDHρ^*, while for $u > 2.6$, F15 $>$ DDH3$\rho\delta^*$ $>$ DDHρ^* $>$ Fa3.

TABLE I: Parameter sets for the nuclear equation of state used in the extended version of the UrQMD model.

EoS	α [MeV]	β [MeV]	$\gamma_{\rm sky}$	$t_{\rm md}$ [MeV]	$a_{\rm md}$ [$\frac{c^2}{\rm GeV^2}$]	S_0 [MeV]
H	-165	126	1.676	-	-	34
S	-353	304	7/6	-	-	34
HM	-138	60	2.08	1.57	500	34
SM	-393	320	1.14	1.57	500	34

3. Momentum-dependent interactions for all baryons are introduced. The form of the momentum dependence is taken from the IQMD model [10, 34], which reads

$$U_{\rm md} = t_{\rm md} \ln^2[1 + a_{\rm md}(\Delta \mathbf{p})^2]u, \tag{1}$$

in which $\Delta \mathbf{p} = \mathbf{p}_i - \mathbf{p}_j$ represents the relative momentum of two nucleons i and j. The parametrizations of $t_{\rm md}$ and $a_{\rm md}$ are listed in Table I. We note that B.-A. Li et al. have used an isospin-dependent momentum-dependent parametrization in the BUU model, which is guided by a Hartree-Fock calculation using the Gogny effective interaction [35, 36]. However, here we do not consider the isospin dependence in the momentum dependent part of the mean field.

Besides the two- and three-body Skyrme potential ($U_{\rm sky} = \alpha\, u + \beta\, u^{\gamma_{\rm sky}}$), similar to the IQMD model [10, 37], we consider a variant nuclear incompressibility, namely, a hard EoS with $K = 300$ MeV ("H-EoS"), a soft EoS with $K = 200$ MeV ("S-EoS"), a hard EoS ($K = 380$ MeV) with momentum dependence ("HM-EoS"), and a soft EoS ($K = 200$ MeV) with momentum dependence ("SM-EoS"). The parameters of the various EoS used in the UrQMD model are listed in Table I. In order to reproduce the ground-state properties of finite nuclei in the UrQMD model (for instance, the binding energy E_B and the r.m.s radius), the parameters have been slightly readjusted. Note, that the potentials used here are not included in the currently available version of the model, but will be included in future versions.

III. RESULTS AND DISCUSSIONS

Firstly, we test the applicability of the UrQMD model to intermediate energy HICs. Fig. 2 shows the results for the excitation function of pion multiplicities in central ($b = 0$ fm) ^{197}Au+^{197}Au reactions at energies from $0.4A$ to $1.5A$ GeV and the comparison with the recent FOPI preliminarily experimental data [38]. The ratios between the calculations (with S- and SM-EoS and without potentials, namely the cascade mode) and the experimental data are shown in the lower plot. In Ref. [39] the multiplicities of pions were compared within various transport approaches for HICs around $1A$ GeV. A significant variation of the total pion yield with the different approaches has been found. Generally, these transport models overpredict the pion yields. Overall, our calculations (Fig. 2 with EoS, especially with a S-EoS) are in good agreement with data, while the results without mean-field potential (the cascade mode) deviate from the experimental data at lower beam energies ($< 0.8A$ GeV).

Now let us turn to see how both the Coulomb and the symmetry potentials influence the production of pions in isospin-symmetric HICs. Fig. 3 shows the rapidity (upper plots) and the transverse momentum (lower plots) distributions (in the center-of-mass system) of pions in central ($b = 0$ fm) collisions ^{40}Ca+^{40}Ca at beam energy $E_b = 0.4A$ GeV. The SM-EoS and the F15 symmetry potential energy are selected here. In the left (right) two plots we show the distributions without (with) the contribution of both Coulomb (of all charged hadrons) and symmetry potentials. When the Coulomb and symmetry potentials are switched off, the multiplicities of π^-, π^+, and π^0 are equal to each other within statistical errors, which means that the isospin symmetry is preserved, as one expects. While the Coulomb and symmetry potentials are switched on, the rapidity and transverse momentum distributions of π^-, π^+, and π^0 mesons are clearly different. At mid-rapidity and in the low transverse momentum region, the multiplicity of π^+ mesons is smaller than the π^- ones, and vice versa in the region of the projectile-target rapidity or large transverse momentum. We notice that, after integrating the multiplicities of π^- and π^+ mesons separately, the π^-/π^+ ratio is about 1.05. We have also checked this ratio at a higher beam energy, $E_{\rm b} = 0.8A$ GeV, and found that it is reduced to 1.02.

Fig. 4 shows the rapidity (upper plot) and the transverse momentum (lower plot) distributions of the π^-/π^+ ratio for the same reaction as in Fig. 3. In the plots we show the results for the following cases (1) without hadronic Coulomb and baryonic symmetry po-

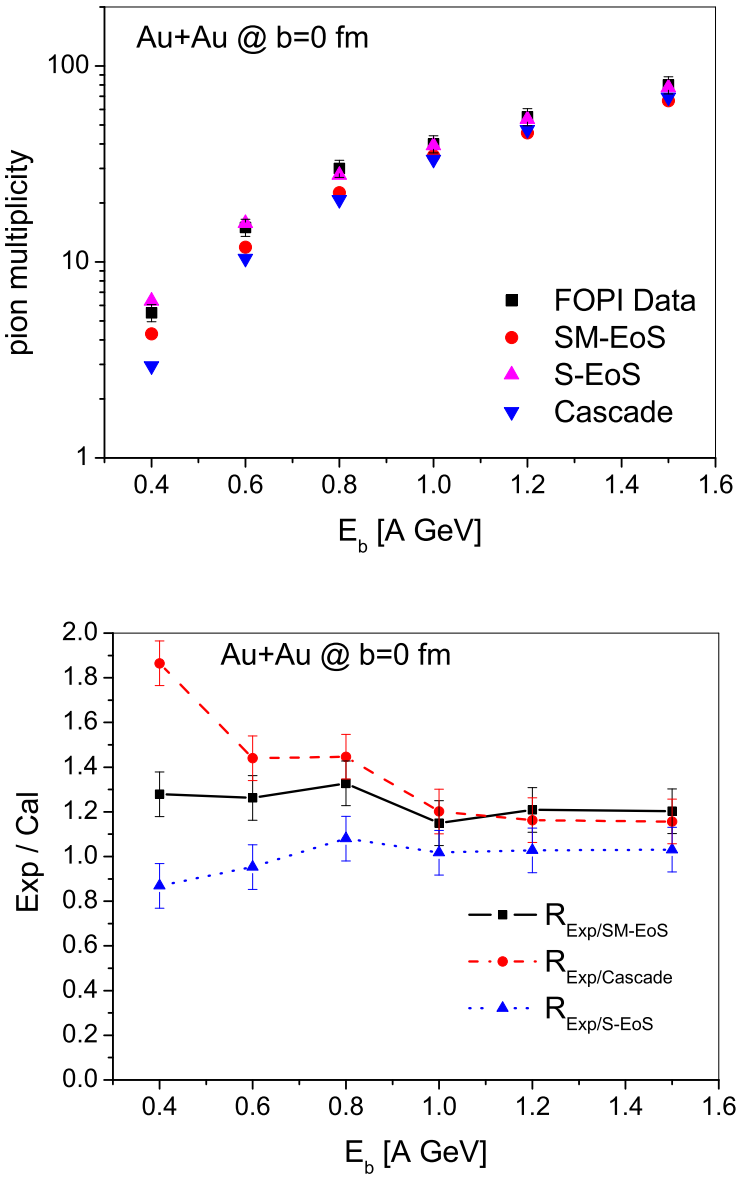

FIG. 2: Upper plot: The excitation function of the pion multiplicities for central (b = 0 fm) ^{197}Au+^{197}Au reaction. The Cascade-mode, S-EoS, and SM-EoS are adopted for calculations. The FOPI preliminary data for central Au+Au collisions are also shown [38]. Lower plot: The ratios between the experimental data and the calculations.

tentials ("No Coul. and Sym. Pot.") (2) with hadronic Coulomb and baryonic symmetry potentials F15 and DDHρ^* ("F15" and "DDHρ^*") and (3) without the hadronic Coulomb potential but with the DDHρ^* symmetry potential energy ("No Coul. Pot."). One finds that without the Coulomb and symmetry potentials the π^-/π^+ ratio is around unity. When the Coulomb and symmetry potentials are switched on, the π^-/π^+ ratio depends weakly on the symmetry potential. At mid-rapidity and at large transverse momenta, the softer the symmetry potential is, the larger the π^-/π^+ ratio is, and the other way around in the regions of projectile-target rapidity and small transverse momentum. When the Coulomb interaction is switched off but the symmetry potential is on, i.e., case (3), the π^-/π^+ ratio is again around unity. This means that the Coulomb interaction is the leading cause of the π^-/π^+ ratio deviating from unity, which is shown in case (2). When the Coulomb potential is taken into account, the protons and also the positively charged Δs are slightly pushed into the lower density region so that more neutrons and negatively charged Δs will be in the high-density region. As a consequence, the isospin asymmetry $(\rho_n - \rho_p)/(\rho_n + \rho_p)$ will be different from zero locally although the total system is isospin-symmetric. Thus, the symmetry potential begins to play a role that leads to the π^-/π^+ ratio depending on the symmetry potential for case (2). So we expect that the deviation of the π^-/π^+ ratio from unity depends on rapidity and transverse momentum and helps to determine the symmetry potential for isospin-symmetric systems.

Before investigating the influence of various mean-field potentials on the pion flow in intermediate energy HICs, it is necessary to show the rapidity distributions of π^- and π^+ mesons (Fig. 5), as well as the π^-/π^+ ratios (Fig. 6). They are calculated (1) with different isospin-independent EoS, that is, the H-, S-, and SM-EoS (left plot, titled "EoS-0") but with the same symmetry potential F15 and including the hadronic Coulomb interaction; 2) with or without mesonic Coulomb potential (middle plot, titled "M-Coul-Pot") but with the same H-EoS and the symmetry potential F15; and (3) with different symmetry potentials F15 and Fa3 (right plot, titled "Sym-Pot") but with the same H-EoS and the hadronic Coulomb potential. Semi-peripheral ($b = 7 - 9$ fm) ^{208}Pb +^{208} Pb collisions at $E_b = 0.8A$ GeV are studied for all following calculations. From Fig. 5 we can see, at first glance, the uncertainty of the isospin-independent EoS obviously affects the total pion multiplicity; the effect of the density dependence of the symmetry potential on the π^- multiplicity is visible, while the mesonic Coulomb potential hardly affects the multiplicity of charged pions in the

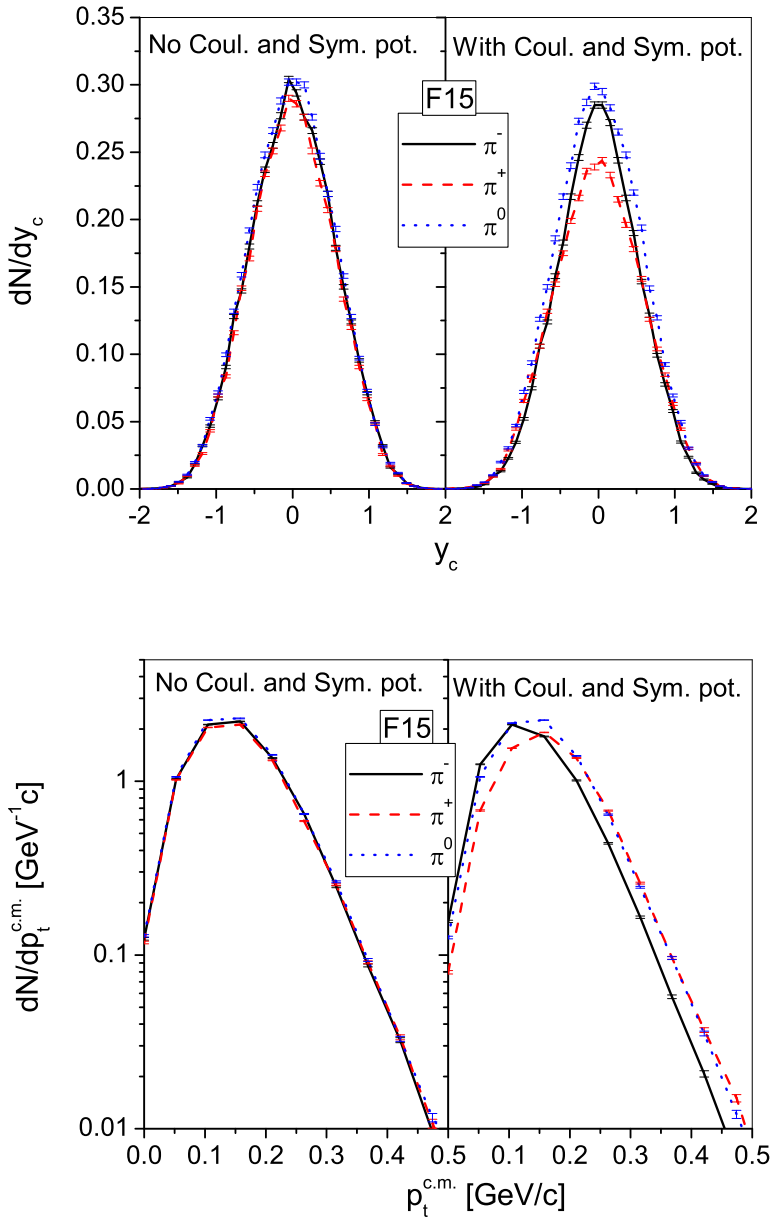

FIG. 3: The rapidity (upper plots) and the transverse momentum (lower plots) distributions of pions with (right plots) or without (left plots) hadronic Coulomb and baryonic symmetry potentials. The isospin-symmetric reaction ^{40}Ca +^{40} Ca at the beam energy $E_b = 0.4A$ GeV with the impact parameter $b = 0$ fm is chosen.

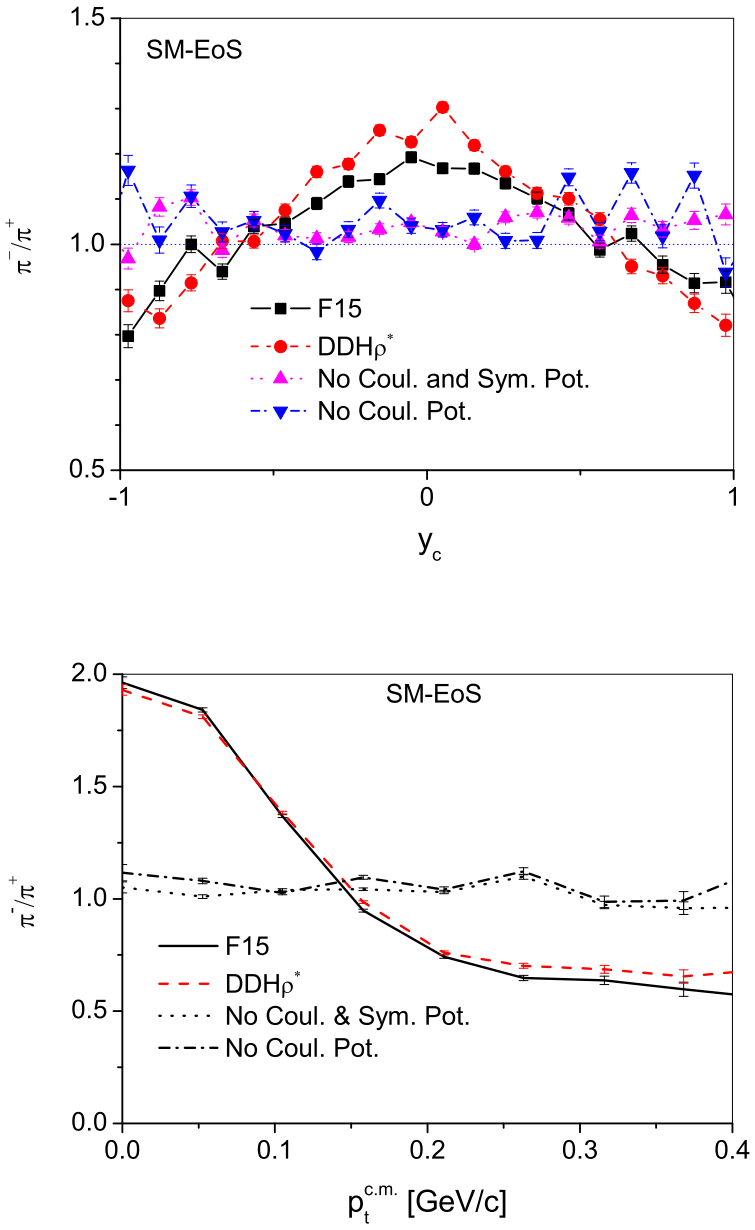

FIG. 4: The rapidity (upper plot) and the transverse momentum (lower plot) distributions of the π^-/π^+ ratio as calculated (1) without symmetry and the Coulomb potentials ("No Coul. and Sym. Pot."); (2) with symmetry and Coulomb potentials (cases "F15" and "DDHρ^*"); and (3) without Coulomb potential but with symmetry potential DDHρ^* ("No Coul. Pot."). The reaction ^{40}Ca $+^{40}$ Ca at $E_b = 0.4A$ GeV with $b = 0$ fm is chosen.

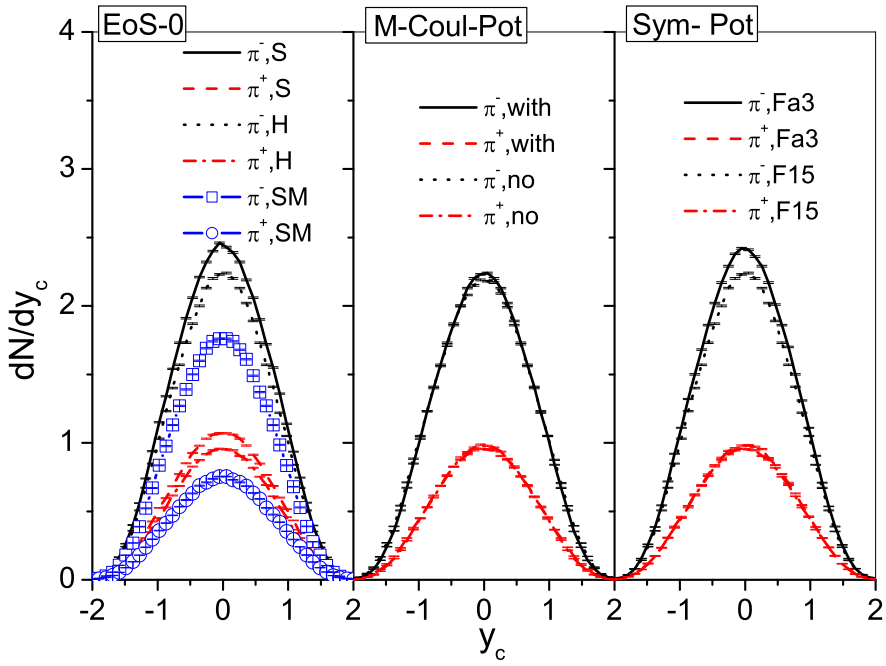

FIG. 5: Rapidity distributions of π^- and π^+ for various isospin-independent EoS (S-, H, and SM-EoS, left plot), with or without mesonic Coulomb potential (middle plot), and with the F15 and Fa3 symmetry potentials (right plot) (see text). The reaction ^{208}Pb $+^{208}$ Pb at $E_b = 0.8A$ GeV and $b = 7 - 9$ fm is chosen.

neutron-rich ^{208}Pb $+^{208}$ Pb system. These characteristics have already been seen in [17]. The left plot of Fig. 5 shows that the pion yield with momentum dependent interactions (SM-EoS) is obviously lower than that with S-EoS or H-EoS, which has been shown in Ref. [7]. Further, we see that both the mesonic Coulomb and the symmetry potentials hardly affect the π^+ multiplicities in neutron-rich HICs. Therefore, the rapidity distribution of π^+ can provide more accurate information on the isospin-independent part of the EoS for the neutron-rich HICs.

The π^-/π^+ ratio at $-1 < y_c < 1$ is smaller for a soft EoS as compared to a hard EoS (left plot of Fig. 6), due to more two-body scatterings. The π^-/π^+ ratio with a soft symmetry potential is larger than the one with a hard symmetry potential (right plot). The effect of the symmetry potential has been studied extensively in [17, 18]. Here we want to stress that both, the isospin-independent and isospin-dependent EoS parts, obviously affect the π^-/π^+

ratio but in the opposite direction when the stiffness changes from soft to hard. When the mesonic Coulomb potential is not taken into account (middle plot) the π^-/π^+ ratio is larger at rapidities exceeding one than at mid-rapidity, which was proven wrong by experimental measurements, for example, see Ref. [24]. It means that the mesonic Coulomb potential needs to be considered, besides the baryonic Coulomb potential. One further finds from this figure that the π^-/π^+ ratio becomes rather flat at small rapidities ($-0.75 < y_c < 0.75$) in the semi-peripheral HICs. We have also found a double peaked structure (in the projectile and target regions) of the rapidity distribution of the π^-/π^+ ratio at even larger impact parameters. This behavior is rather different from central collisions (upper plot of Fig. 4) where the π^-/π^+ ratio is peaked in the mid-rapidity region. This change of the behavior of the π^-/π^+ ratio as a function of rapidity from central to semi-peripheral HICs is due to the decrease of the number of nucleon-nucleon collisions [7, 15].

Now let us turn to discuss collective flow observables. Fig. 7 shows the in-plane directed transverse flow of charged pions as a function of rapidity. It is well known that the directed flow of particles is particularly sensitive to the stiffness of the EoS, which is also shown in the left plot of Fig. 7. The weak anti-flow of charged pions for semi-peripheral collisions is well reproduced, similar to the calculations and the experiments in Refs. [10, 19, 22] for semi-peripheral Au+Au collisions at different beam energies. Among the three types of the EoS studied here, the anti-flow effect of π^- and π^+ calculated with the SM-Eos is the strongest, followed by the S-EoS [10]. The anti-flow effect of π^+ is much stronger than that of π^-. If the mesonic Coulomb potential is neglected, the absolute value of the antiflow parameter of π^- is even higher than that of π^+ as shown in the middle of Fig. 7, which is in disagreement with experimental measurements [22]. In the right plot of Fig. 7, we find that the effect of the density dependence of the symmetry potential on the charged pion flow is very weak, which means that the in-plane directed flow of charged pions can provide more accurate information on the isospin-independent part of the EoS rather than on the isospin dependent part.

In Fig. 8 we show the rapidity distributions of the π^+-π^- transverse flow difference $\Delta p_x^{\rm pm}$ defined by $\Delta p_x^{\rm pm} = p_x^{\pi^+} - p_x^{\pi^-}$. $p_x^{\rm pm}$ is similar when calculated with S-EoS, H-EoS as well as SM-EoS at mid-rapidity, but it turns out to be different between with the momentum dependence (SM-EoS) and without the momentum dependence (S-EoS and H-EoS) in the projectile-target rapidity region. Again, from the right plot we find that $\Delta p_x^{\rm pm}$ depends

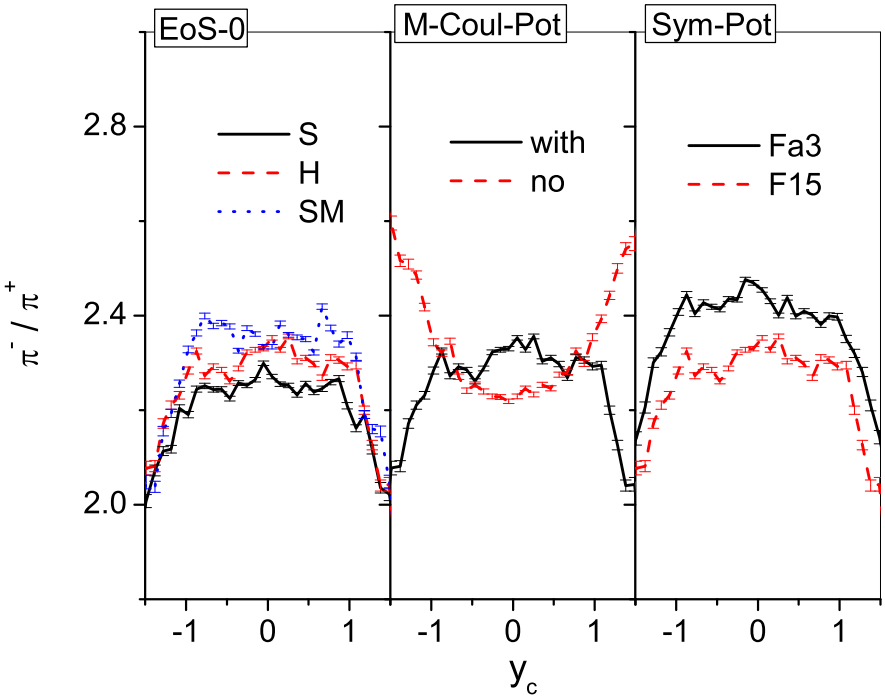

FIG. 6: Rapidity distributions of π^-/π^+ ratios for various isospin-independent EoS (S-, H, and SM-EoS, left plot), with or without mesonic Coulomb potential (middle plot), and with the F15 and Fa3 symmetry potentials (right plot) (see text). The reaction ^{208}Pb +^{208} Pb at $E_b = 0.8A$ GeV and $b = 7 - 9$ fm is chosen.

only weakly on the symmetry potential. Thus, we conclude that the π^+-π^- transverse flow difference $\Delta p_x^{\rm pm}$ can be adopted to probe the momentum dependence of the EoS.

Fig. 9 shows the influence of different parts in the EoS on the π^+-π^- elliptic flow difference as a function of rapidity, which is defined as $\Delta v_2^{\rm pm} = v_2^{\pi^+} - v_2^{\pi^-}$. Here $v_2 = \langle (\frac{p_x}{p_t})^2 - (\frac{p_y}{p_t})^2 \rangle$ and $v_2^{\pi^+}$ is the elliptic flow for π^+, $v_2^{\pi^-}$ is the elliptic flow for π^-. First, we see that $\Delta v_2^{\rm pm}$ value is always negative when the mesonic Coulomb interaction is taken into account. The influence of the mesonic Coulomb interaction on the π^+-π^- elliptic flow difference is shown in the middle plot of Fig. 9. $\Delta v_2^{\rm pm}$ is almost zero when the mesonic Coulomb interaction is switched off. When the mesonic Coulomb interaction is switched on, the out-of-plane elliptic flow becomes larger for π^+ than for π^- mesons which leads to a negatively elliptic flow difference. The left and right plots of Fig. 9 show that $\Delta v_2^{\rm pm}$ is insensitive to the uncertainties of both the isospin-independent and -dependent parts of the EoS. The effect of the momentum

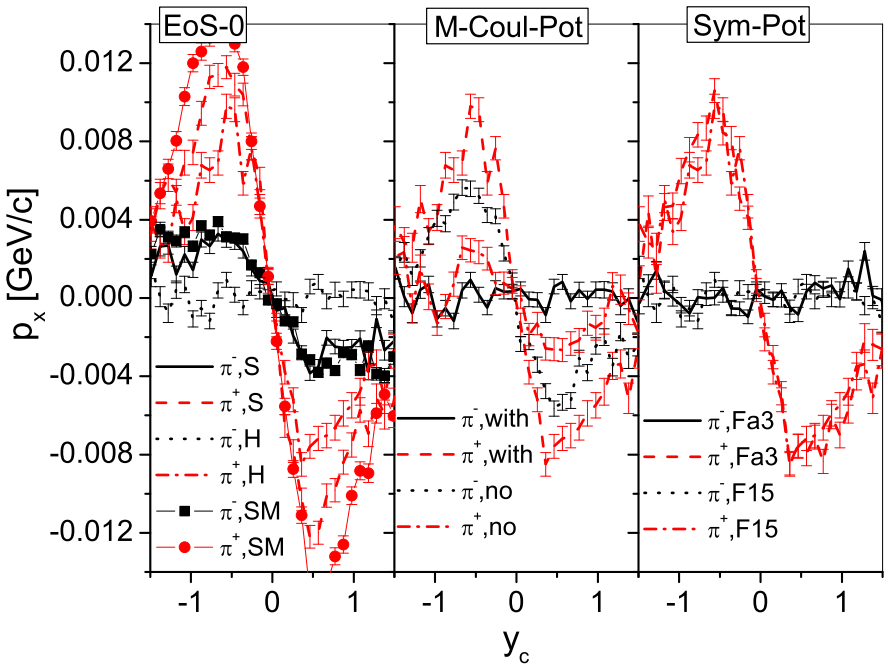

FIG. 7: The directed transverse flow distributions of the π^- and π^+ mesons for various isospin-independent EoS (S-, H, and SM-EoS, left plot), with or without mesonic Coulomb potential (middle plot), and with the F15 and Fa3 symmetry potentials (right plot) (see text). The reaction ^{208}Pb $+^{208}$ Pb at $E_b = 0.8A$ GeV and $b = 7 - 9$ fm is chosen.

dependence of the EoS has only little effect on $\Delta v_2^{\rm pm}$. The weak dependence of the rapidity distribution of $\Delta v_2^{\rm pm}$ on the mean-field potentials might be useful for extracting exclusive information on medium corrections of the binary cross sections.

From the above discussions on the pion flow (Figs. 7-9), one might have the impression that the pion flow is not sensitive to the density dependence of the symmetry potential. Actually, this is not true, when we study the *transverse momentum* dependence of $\Delta v_2^{\rm pm}$. In Fig. 10 we illustrate $\Delta v_2^{\rm pm}$ of charged *pions* as a function of transverse momentum $p_t^{c.m.}$. The SM-EoS is adopted in the calculations. $\Delta v_2^{\rm pm}$ is negative for all $p_t^{c.m.}$. The dependence of $\Delta v_2^{\rm pm}$ on the form of the density dependence of the symmetry potential becomes very pronounced at large transverse momenta $\sim 0.2 - 0.5$ GeV/c. This behavior is very similar to the proton and neutron elliptic flow difference $v_2^{\rm pn}$ [32, 40]. As it is known that pions with high transverse momenta are mainly produced from the high density region, Comparing

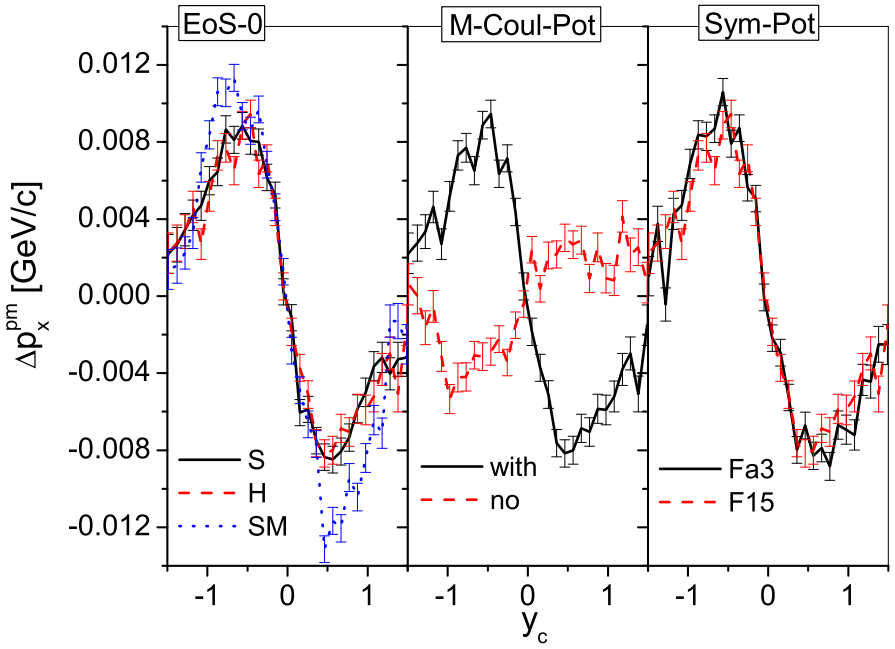

FIG. 8: The rapidity distributions of the $\pi^+ - \pi^-$ transverse flow difference ($\Delta p_x^{\rm pm} = p_x^{\pi^+} - p_x^{\pi^-}$) for various isospin-independent EoS (S-, H, and SM-EoS, left plot), with or without mesonic Coulomb potential (middle plot), and with the F15 and Fa3 symmetry potentials (right plot) (see text). The reaction ^{208}Pb $+^{208}$ Pb at $E_b = 0.8A$ GeV and $b = 7 - 9$ fm is chosen.

Fig. 10 with Fig. 1, we deduce that it reflects explicitly the density dependence of the symmetry potential at densities $u > 1$. At densities $u > 2.6$ (Fig. 1) the symmetry potential Fa3 is smaller than DDHρ^* which is also reflected in Fig. 10 at the transverse momentum ~ 0.5 GeV/c. At higher transverse momenta, although more than 1.6 million events were calculated, the statistical errors are quite large and the results are not shown here.

IV. SUMMARY AND OUTLOOK

In summary, based on the UrQMD model (version 1.3) we have studied the influence of different parts of the EoS such as the isospin-independent, the Coulomb interaction (the Coulomb interaction between meson and meson (baryon) is also considered) and the symmetry energy on a variety of observables related to pion production in intermediate energy HICs. We first have studied the isospin-symmetric central ^{40}Ca $+^{40}$ Ca collisions. It shows

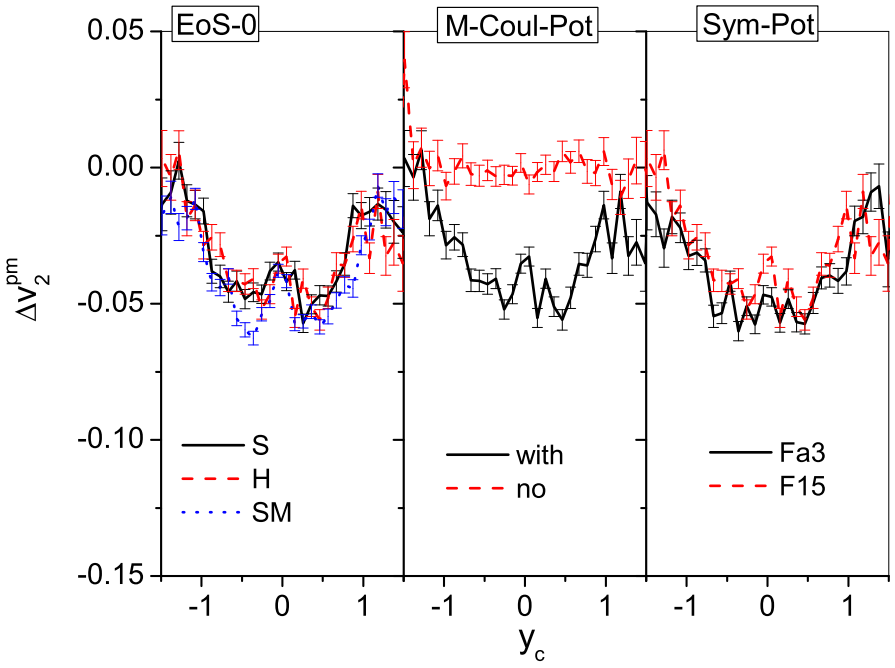

FIG. 9: Rapidity distributions of the $\pi^+ - \pi^-$ elliptic flow difference ($\Delta v_2^{\rm pm} = v_2^{\pi^+} - v_2^{\pi^-}$) for various isospin-independent EoS (S-, H, and SM-EoS, left plot), with or without mesonic Coulomb potential (middle plot), and with the F15 and Fa3 symmetry potentials (right plot) (see text). The reaction ^{208}Pb +^{208} Pb at $E_b = 0.8A$ GeV and $b = 7 - 9$ fm is chosen.

that the Coulomb interaction plays an important role in the reaction dynamics and influences the rapidity and transverse momentum distributions of charged pions considerably. Due to the effect of the Coulomb potential, the π^-/π^+ ratio deviates from unity and shows the dependence on the symmetry potential even for isospin-symmetric systems. Our study shows that the rapidity distributions of the pions and the π^-/π^+ ratio are strongly influenced by the uncertainty of the EoS, while positively charged pions from neutron-rich HICs are much less influenced by the density dependence of the symmetry potential.

We have also studied the pion directed and elliptic flow (difference) as functions of rapidity and transverse momentum for the neutron-rich system ^{208}Pb +^{208} Pb. We find that the mesonic Coulomb interaction plays an important role in reproducing the proper pion flow. The omission of mesonic Coulomb interaction leads to a wrong behavior of the rapidity distribution of the π^-/π^+ ratio and the charged pion directed and elliptic flow. We have also

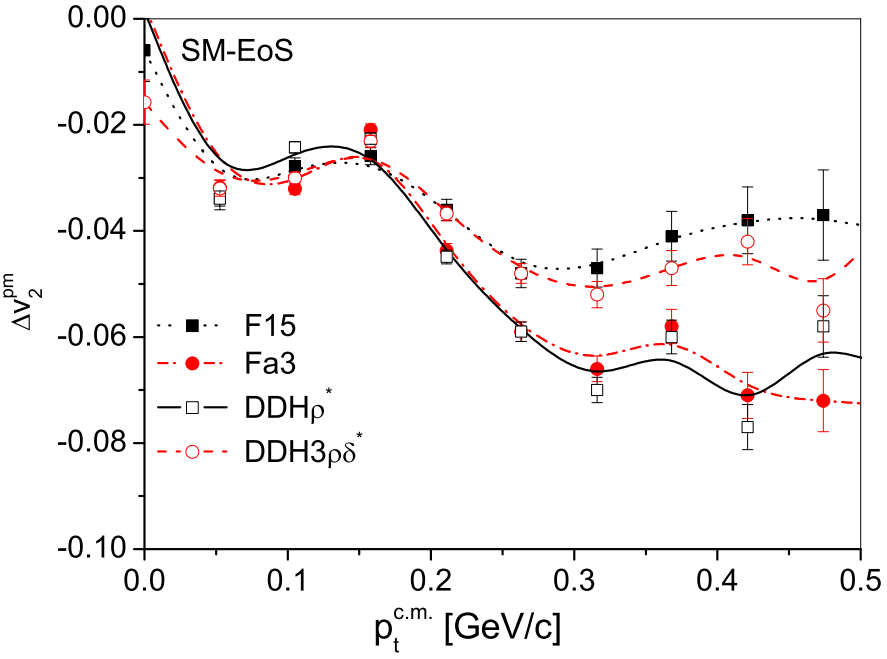

FIG. 10: The transverse momentum distribution of the $\Delta v_2^{\rm pm}$ with different symmetry potentials. The SM-EoS is adopted for the ^{208}Pb $+^{208}$ Pb reaction at $E_b = 0.8A$ GeV and $b = 7 - 9$ fm.

found that the directed flow is sensitive to the isospin-independent EoS but not sensitive to the various forms of the density dependence of the symmetry potential. The rapidity distribution of the transverse flow difference $\Delta p_x^{\rm pm}$ of charged pions shows the sensitivity only to the momentum dependence of the EoS. The rapidity distribution of the elliptic flow difference $\Delta v_2^{\rm pm}$ of charged pions is insensitive to the mean field potentials. However, the transverse momentum distribution of $\Delta v_2^{\rm pm}$ of charged pions (at transverse momenta $\sim 0.2-0.5$ GeV/c) becomes more sensitive to the form of the density dependence of the symmetry potential. Thus, we can use the extensive comparison of multiple observables between the calculations and the intermediate-energy experimental data to extract comprehensive information on the EoS.

Acknowledgments

Q. Li thanks the Alexander von Humboldt-Stiftung for a fellowship. This work is partly supported by the National Natural Science Foundation of China under Grant No. 10235030

and the Major State Basic Research Development Program of China under Contract No. G20000774, as well as by GSI, BMBF, DFG, and Volkswagenstiftung.

---

[1] D. Vretenar, T. Niksic, and P. Ring, Phys. Rev. C **68**, 024310 (2003).

[2] J. Rizzo, M. Colonna, M. Di Toro, and V. Greco, Nucl. Phys. A. **732**, 202 (2004).

[3] M. B. Tsang, W. A. Friedman, C. K. Gelbke, W. G. Lynch, G. Verde, and H. Xu, Phys. Rev. Lett. **86**, 5023 (2001).

[4] R. J. Furnstahl, Nucl. Phys. A **706**, 85 (2002).

[5] L. W. Chen, C. M. Ko, and B.-A. Li, Phys. Rev. Lett. **94**, 032701 (2005).

[6] Dao T. Khoa and Hoang Sy Than, nucl-th/0502059.

[7] J. Aichelin, A. Rosenhauer, G. Peilert, H. Stöcker, and W. Greiner, Phys. Rev. Lett. **58**, 1926 (1987).

[8] C. Gale, G. M. Welke, M. Prakash, S. J. Lee, and S. Das Gupta, Phys. Rev. C **41**, 1545 (1990).

[9] M. D. Partlan *et al.*, Phys. Rev. Lett. **75**, 2100 (1995).

[10] S. A. Bass, C. Hartnack, H. Stöcker, and W. Greiner, Phys. Rev. C **51**, 3343 (1995).

[11] V. Greco, A. Guarnera, M. Colonna, and M. Di Toro, Phys. Rev. C **59**, 810 (1999).

[12] B.-A. Li, G.-C Yong, and W. Zuo, Phys. Rev. C **71**, 014608 (2005).

[13] P. Danielewicz, Nucl. Phys. A **673**, 375 (2000).

[14] P. Danielewicz, Nucl. Phys. A **685**, 368 (2001).

[15] V. S. Uma Maheswari, C. Fuchs, A. Faessler, Z. S. Wang, and D. S. Kosov, Phys. Rev. C **57**, 922 (1998).

[16] A. Wagner *et al.*, Phys. Rev. Lett. **85**, 18 (2000).

[17] Q. Li, Z. Li, S. Soff, M. Bleicher, H. Stöcker, accepted by J. Phys. G.

[18] Q. Li, Z. Li, E. Zhao, and R. K. Gupta, Phys. Rev. C **71**, 054907 (2005).

[19] B.-A. Li and C. M. Ko, Phys. Rev. C **53**, R22 (1996).

[20] B.-A. Li, C. M. Ko, A. T. Sustich, and Bin Zhang, Phys. Rev. C **60**, 011901(R) (1999).

[21] L. V. Bravina, A. Faessler, C. Fuchs, and E. E. Zabrodin, Phys. Rev. C **61**, 064902 (2000).

[22] J. C. Kintner *et al.*, Phys. Rev. Lett. **78**, 4165 (1997).

[23] FOPI Collaboration, D. Pelte *et al.*, Z. Phys. A **357**, 215 (1997); *ibid*, A **359**, 55 (1997).

[24] FOPI Collaboration, B. Hong *et al.*, Phys. Rev. C **71**, 034902 (2005).

[25] S. A. Bass *et al.*, Prog. Part. Nucl. Phys. **41**, 255 (1998).

[26] M. Bleicher *et al.*, J. Phys. G: Nucl. Part. Phys. **25**, 1859 (1999).

[27] M. Reiter, E. L. Bratkovskaya, M. Bleicher, W. Bauer, W. Cassing, H. Weber, and H. Stöcker, Nucl. Phys. A **722**, 142 (2003).

[28] E. L. Bratkovskaya, M. Bleicher, M. Reiter, S. Soff, H. Stöcker, M. van Leeuwen, S. A. Bass, W. Cassing, Phys. Rev. C **69**, 054907 (2004).

[29] J. Aichelin, Phys. Rep. **202**, 233 (1991).

[30] S. Soff, S. A. Bass, M. Bleicher, H. Stöcker, W. Greiner, nucl-th/9903061.

[31] B.-A. Li, Phys. Rev. Lett. **88**, 192701 (2002).

[32] T. Gaitanos, M. Di Toro, G. Ferini, M. Colonna, and H. H. Wolter, nucl-th/0402041.

[33] E. N. E. van Dalen, C. Fuchs, and Amand Faessler, Nucl. Phys. A **744** 227 (2004).

[34] J. Aichelin, A. Rosenhauer, G. Peilert, H. Stöcker, and W. Greiner, Phys. Rev. Lett. **58**, 1926 (1987).

[35] B.-A. Li, C. B. Das, S. D. Gupta, and C. Gale, Phys. Rev. C **69**, 011603(R) (2004).

[36] B.-A. Li, C. B. Das, S. D. Gupta, and C. Gale, Nucl. Phys. A **735**, 563 (2004).

[37] S. Soff, S. A. Bass, C. Hartnack, H. Stöcker, and W. Greiner, Phys. Rev. C **51**, 3320 (1995).

[38] W. Reisdorf, FOPI collaboration, preliminary data.

[39] E. E. Kolomeitsev, C. Hartnack, H. W. Barz, M. Bleicher, E. Bratkovskaya, W. Cassing, L. W. Chen, P. Danielewicz, C. Fuchs, T. Gaitanos, C. M. Ko, A. Larionov, M. Reiter, Gy. Wolf, J. Aichelin, J. Phys. G **31**, S741 (2005).

[40] V. Greco, V. Baran, M. Colonna, M. Di Toro, T. Gaitanos, and H. H. Wolter, Phys. Lett. B **562** 215 (2003).